Original Article

VasoMetrics: unbiased spatiotemporal analysis of microvascular diameter in multi-photon imaging applications

Konnor P. McDowell[1], Andrée-Anne Berthiaume[1,2], Taryn Tieu[1], David A. Hartmann[3], Andy Y. Shih[1,4,5]

[1]Center for Developmental Biology and Regenerative Medicine, Seattle Children's Research Institute, Seattle, WA, USA; [2]Department of Neuroscience, Medical University of South Carolina, Charleston, SC, USA; [3]Department of Neurology & Neurological Sciences, Stanford University School of Medicine, Stanford, CA, USA; [4]Department of Pediatrics, University of Washington, Seattle, WA, USA; [5]Department of Bioengineering, University of Washington, Seattle, WA, USA

Correspondence to: Andy Y. Shih. Center for Developmental Biology and Regenerative Medicine, Seattle Children's Research Institute, Seattle, WA, USA; Department of Pediatrics, Department of Bioengineering, University of Washington, Seattle, WA, USA. Email: Andy.Shih@SeattleChildrens.org.

Background: Multi-photon imaging of the cerebrovasculature provides rich data on the dynamics of cortical arterioles, capillaries, and venules. Vascular diameter is the major determinant of blood flow resistance, and is the most commonly quantified metric in studies of the cerebrovasculature. However, there is a lack of accessible and easy-to-use methods to quantify vascular diameter in imaging data.

Methods: We created VasoMetrics, a macro written in ImageJ/Fiji for spatiotemporal analysis of microvascular diameter. The key feature of VasoMetrics is rapid analysis of many evenly spaced cross-sectional lines along the vessel of interest, permitting the extraction of numerous diameter measurements from individual vessels. Here we demonstrated the utility of VasoMetrics by analyzing *in vivo* multi-photon imaging stacks and movies collected from lightly sedated mice, as well as data from optical coherence tomography angiography (OCTA) of human retina.

Results: Compared to the standard approach, which is to measure cross-sectional diameters at arbitrary points along a vessel, VasoMetrics accurately reported spatiotemporal features of vessel diameter, reduced measurement bias and time spent analyzing data, and improved the reproducibility of diameter measurements between users. VasoMetrics revealed the dynamics in pial arteriole diameters during vasomotion at rest, as well as changes in capillary diameter before and after pericyte ablation. Retinal arteriole diameter was quantified from a human retinal angiogram, providing proof-of-principle that VasoMetrics can be applied to contrast-enhanced clinical imaging of microvasculature.

Conclusions: VasoMetrics is a robust macro for spatiotemporal analysis of microvascular diameter in imaging applications.

Keywords: Vasculature; diameter; multi-photon imaging; brain; retina; angiogram

Submitted Jul 31, 2020. Accepted for publication Nov 17, 2020.
doi: 10.21037/qims-20-920
View this article at: http://dx.doi.org/10.21037/qims-20-920

Introduction

In vivo multi-photon imaging is a common preclinical technique to study the 3-D architecture of microvascular networks and the perfusion of blood vessels in the living brain (1). Cerebral blood flow must be constantly and carefully regulated because the brain lacks its own energy reserve. The diameter of the vascular lumen is one major determinant of blood flow resistance, and as such, vessel diameter is modulated to best serve the energetic demands of surrounding neurons and other brain cell types (2). Neurally-evoked modulation of arteriole diameter (neurovascular coupling) is crucial for on-demand local supply of oxygen and nutrients to brain cells during periods of activity. This process is overlaid on slow ongoing

oscillations in diameter under basal conditions (3,4). Below the brain surface, the vast majority of vascular length is composed of tortuous capillary networks, where even miniscule changes in capillary diameter can profoundly influence blood flow. Recent studies have shown that capillary flow rates homogenize to improve oxygen and nutrient delivery during functional hyperemia, suggesting that this process may involve fine adjustments in capillary diameter to modulate red blood cell (RBC) passage (5-7).

In a typical multi-photon study of brain vasculature, imaging is performed through a cranial window in an anesthetized or awake rodent. The vasculature is labeled by intravenous injection of a high molecular weight fluorescent dye (8). Data are then collected as single images or image z stacks for snapshots of vascular structure, or sequential images (movies) to assess spatiotemporal dynamics. Measurements of vascular diameter in these data have been performed manually using image analysis software such as ImageJ/Fiji (9), where the user defines the location of the vessel wall edges and measures the distance between these edges. However, this approach can be prone to error as the precise location of the vessel edge is often difficult to pinpoint. The problem can be addressed by obtaining the fluorescence intensity profile across the vessel lumen, and then quantifying the full-width at half-maximum (FWHM) of this intensity profile for a less subjective measure of vessel diameter (10). Similar algorithms have been used to locate the point of sharpest fluorescence decrease along the vessel wall for unbiased measurement (11). Another approach has been to binarize the image of pial vessels and divide vessel area by vessel length to deduce vessel diameter (12). All these approaches are effective for quantifying vascular diameter, but are limited in two ways. First, they assume that the entire vascular length of interest is undergoing the same degree of change. Second, they are generally implemented by custom-written codes that are less accessible to other researchers.

Vascular diameter is heterogeneous and the dynamics of dilation and contraction may occur unevenly across a single vessel segment. For instance, during neurally-evoked arteriole dilation, the stimulation of a sensory representation such as the forelimb will produce a center-surround effect, where arterioles at the epicenter of neuronal activity dilate, while arterioles of surrounding regions predominantly constrict (13). This is necessary for efficient allocation of blood across the cortex. Another example is in the case of pericytes in the capillary bed, which tend to constrict near their soma in response to stimuli such as pharmacological activation or exposure to hypoxic conditions (14,15). Thus, the location to collect a diameter measurement along a vascular segment has a critical effect on outcome, and poorly chosen locations would both increase measurement bias and overlook relevant biological effects. To address this issue, we created a macro in ImageJ/Fiji that collects vessel intensity profiles at multiple, evenly spaced locations along a user-defined length of vasculature. This enables FWHM diameter to be calculated along an entire vascular segment, and spatiotemporal variation of vessel diameter can be examined in greater detail. It further allows all values across the entire vessel to be averaged together for a single, representative diameter of a given vessel segment. We show that the approach can be used to produce rich data sets of vasomotor responses in pial vessels, and also to study diameter changes in the capillary bed following loss of pericyte coverage.

Methods

Mice

TdTomato reporter mice (Ai14) on a C57BL/6 background were purchased from Jackson Labs (stock no. 007914) (16). These mice were bred with constitutive PDGFRβ-Cre mice (17) to express tdTomato in all mural cells (18). Mice were maintained in standard cages on a 12-hour light-dark cycle, and housed 5 or less per cage. Following cranial window implantation, PDGFRβ-tdTomato mice were housed singly. Mice were between 5 to 7 months of age at the start of imaging. This study was approved by The Institutional Animal Care and Use Committee at the Seattle Children's Research Institute.

Surgery

Cranial imaging windows (1,19) were generated under guidance of a stereoscope (SXZ10; Olympus). Anesthesia was induced with isoflurane (Patterson Veterinary) at 4% mean alveolar concentration in 100% oxygen and maintained at 1–2% during surgery. Body temperature was maintained at 37 ℃ with a feedback-regulated heat pad (FHC Inc.). For analgesia, all animals were administered buprenorphine prior to or immediately following the surgery at a concentration of 0.05 mg/kg. The windows were ~3 mm in diameter and placed over the somatosensory cortex, i.e., windows were centered at 2 mm posterior and 3 mm lateral to Bregma. For imaging of pial arteriole

vasodynamics, we generated polished and reinforced thinned-skull windows, as previously described (19,20). For capillary imaging and pericyte ablation experiments, we generated chronic, skull-removed windows using methods previously described (21).

In vivo two-photon imaging

Imaging was performed with a Bruker Investigator and a Spectra-Physics Insight X3 laser source. For studies examining arteriolar vasodynamics, chlorprothixene sedation was used. We injected 30 µL of 1 mg/mL chlorprothixene solution intramuscularly (thigh muscle), immediately after cranial window surgery with isoflurane (Sigma C1671). We then injected 2 MDa FITC-dextran (FD2000S; Sigma-Aldrich) retro-orbitally under 2% isoflurane, turned off the isoflurane, and waited 15–30 minutes for chlorprothixene to take effect. FITC-dextran was prepared at a concentration of 5% (w/v) and 0.03 mL was injected. For studies examining capillary diameter, mice were imaged under isoflurane anesthesia (~1.25% MAC in medical air), which leaves the mouse anesthetized but reactive to light toe pinch during imaging. In isoflurane experiments, 2 MDa FITC-dextran was also used for vascular labeling. Body temperature was maintained at 37 ℃ with a feed-back regulated heat pad. *In vivo* imaging of FITC-dextran was performed at 800-nm excitation. High-resolution imaging of microvasculature was performed using a 20-X, 1.0 NA water-immersion objective lens (Olympus XLUMPLFLN 20XW). Lateral sampling (x, y) was ~1 µm/pixel (arterioles) or 0.5 µm/pixel (capillaries), and axial sampling (z) was 1 µm/pixel. All lumen diameter quantifications were made in the lateral plane. When imaging with the 20-X objective, laser power ranged between 20–100 mW at the sample, with higher powers required for greater cortical depth. To ablate a single capillary pericyte, a restricted line-scan was applied to only the soma of the target pericyte for ~60 seconds at a power of ~50 mW and excitation wavelength of 725-nm, as previously described (22).

VasoMetrics

The latest version of VasoMetrics macro can be downloaded from a GitHub repository located at https://github.com/mcdowellkonnor/ResearchMacros. A readme file is available to guide the user for macro installation and analysis procedures. Issues, feature suggestions, and code suggestions can be logged through the GitHub repository. Important updates to VasoMetrics will prompt update requests on the user's ImageJ after the macro is launched.

Diameter measurement

The data file to be analyzed is first opened in ImageJ/Fiji. After installing the VasoMetrics macro, a toggle with the symbol "V" on the toolbar of the GUI interface initiates the macro. The user should ensure that the scale of the data is properly set. After an image is opened, the scale of the image can be adjusted by clicking "Analyze" and then "Set Scale…" VasoMetrics will report measurements in the scale provided on the "Set Scale…" menu.

Length and spacing of cross-lines

The program first surveys the data to determine whether the image provided is a single frame, or composed of multiple slices over increasing depth (image stack). If the latter, the image is maximally projected prior to display of a prompt to draw a line along the central axis of the vessel segment to be analyzed ("through-line"). The code then provides an estimate of initial vessel diameter to decide the length of subsequent cross-lines for vessel diameter measurement. The automatic length is determined by drawing a long line perpendicular to the first through-line segment, calculating the FWHM for that line and then adding padding equal to 65% of that FWHM. If a cross-line length cannot be estimated, the user is prompted for this information. Once the trajectory of the through-line is generated, the user is prompted for the spacing of the cross-lines to distribute across the through-line. The default setting provides cross-lines spaced evenly with 5-pixel intervals. The spacing is consistent across through-line segments, allowing the user to contour the through-line appropriately to fit the vessel.

FWHM calculation

Once the cross-lines are generated, the program will take the fluorescence intensity profile of each cross-line. The intensity profile is normalized by subtracting the minimum value from all values in the intensity profile, and then dividing each value by the maximum of all values. The macro first calculates and saves the half-maximum intersection of the normalized intensity profile for each cross-line. The two half-maximum locations closest to the midpoint of the cross-line are considered as likely edges of the vessel of interest. Before obtaining the diameter measurement, the intensity

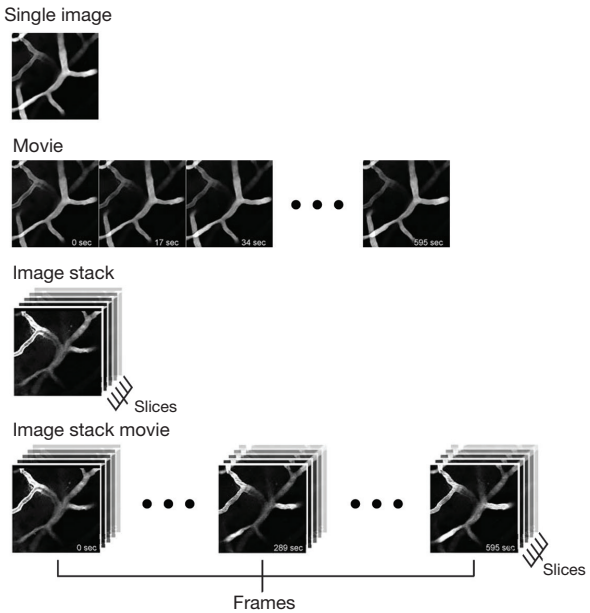

Figure 1 Image formats handled by VasoMetrics. VasoMetrics processes a variety of data types, including single images, image stacks, movies and image stack movies.

profile may be trimmed along the outer edges to remove unnecessary data. The trimming is performed by finding the y intercepts of the derivative of the intensity profile. Data that exists outside of the nearest y intercept of the derivative, respective to the location of the half max intersections closest to the mid-line, is removed. The half-max intersections that are nearest the position of the center of the cross-line are then used for the FWHM diameter calculation. The macro demands a positive slope on the left of the midline and a negative slope on the right, consistent with the intensity profile of only a single vessel. This process helps to remove some erroneous results that might arise if neighboring vessels are touched by the cross-line, or if shadows caused by RBCs are within the lumen. However, this post-processing is not perfect for detection of all potential issues, and the user is advised to check the intensity profiles when possible to detect issues with poorly placed cross-lines. The FWHM is then measured from each of the intensity profiles, with an added interpolation to precisely locate the 0.5 value on either side of the normalized intensity profile to achieve subpixel accuracy. This process is iterated for each cross-line and for each frame.

Outliers and unwanted cross-lines

If possible, vascular branches and areas with significant noise or lack of data should be avoided in the range of the through-line, as full-width half-max data collection may still occur at those areas. Since the FWHM diameter for each individual cross-line is automatically provided along with the average FWHM for the entire segment, any outliers caused by these issues can be identified and excluded from further analyses after moving the data to software such as Microscoft Excel. The identification and exclusion of potential outliers is based on user discretion, as definitions for outliers may differ between users. To re-obtain a mean diameter, unwanted cross-lines can be deleted manually in the region of interest (ROI) manager and the macro re-run with remaining cross-lines. Additionally, movement artifacts in movies can sometimes displace the target vessel from the cross-line position. Therefore, any shifts in the target vessel need to be corrected during pre-processing. This can be achieved with image registration plugins for ImageJ/Fiji, such as StackReg.

Results

VasoMetrics is able to process TIFF files collected in a variety of formats by multi-photon imaging, ranging from single images and movies to 3-D image stacks collected individually or serially over time (image stack movie) (*Figure 1*). The sequence of coded instructions implemented by the macro is outlined in *Figure 2*. The analysis considers two

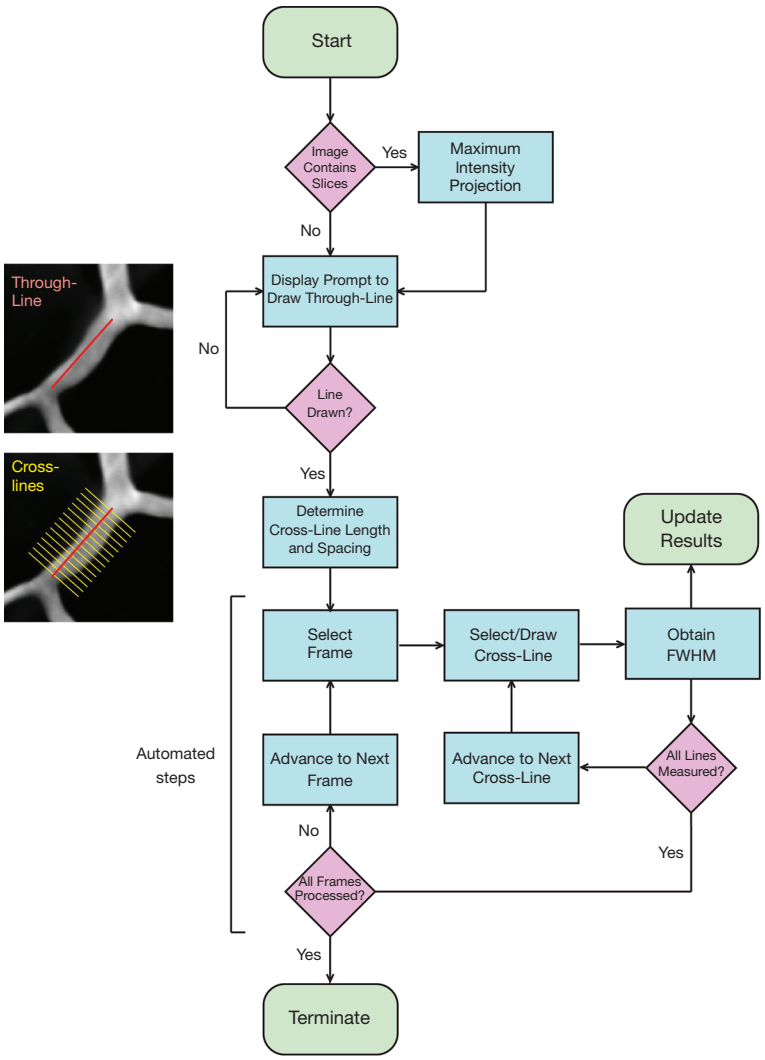

Figure 2 Flow chart for coded instructions implemented by VasoMetrics. VasoMetrics prompts the user for a through-line to define the range over which cross-lines will be placed. Cross-lines provide the fluorescence signal profile across the vessel width for FWHM diameter calculation. The code iterates this process through all cross-lines and all frames until all FWHM measurements have been made. FWHM, full-width at half-maximum.

line types, placed relative to the vessel targeted for analysis. The "through-line" is user-defined, and is drawn along the central axis of the vessel lumen to define the length of vessel over which diameter measurements should be sampled. Subsequently, "cross-lines" are generated automatically by the macro to run perpendicular to the through-line. Cross-lines are numerous and evenly spaced, allowing extraction of diameter over the entire range of the through-line. The user can enter a specific cross-line length, or choose an optimal length automatically calculated by the macro. The user can also change the spacing between cross-lines to alter their density, and thus the total number of diameter measurements obtained from the target vessel. Additional considerations for through and cross-lines are provided in the "Methods" section.

The fluorescence intensity along each cross-line is used to estimate the lumen diameter. When fluorescence intensity is plotted as a function of distance along a single cross-line, the intensity profile typically has a "mesa-like" shape, i.e., flattened peak and sharp decreases in intensity at the vessel wall (*Figure 3A,B*). After normalization of the intensity profile to the maximum and minimum values,

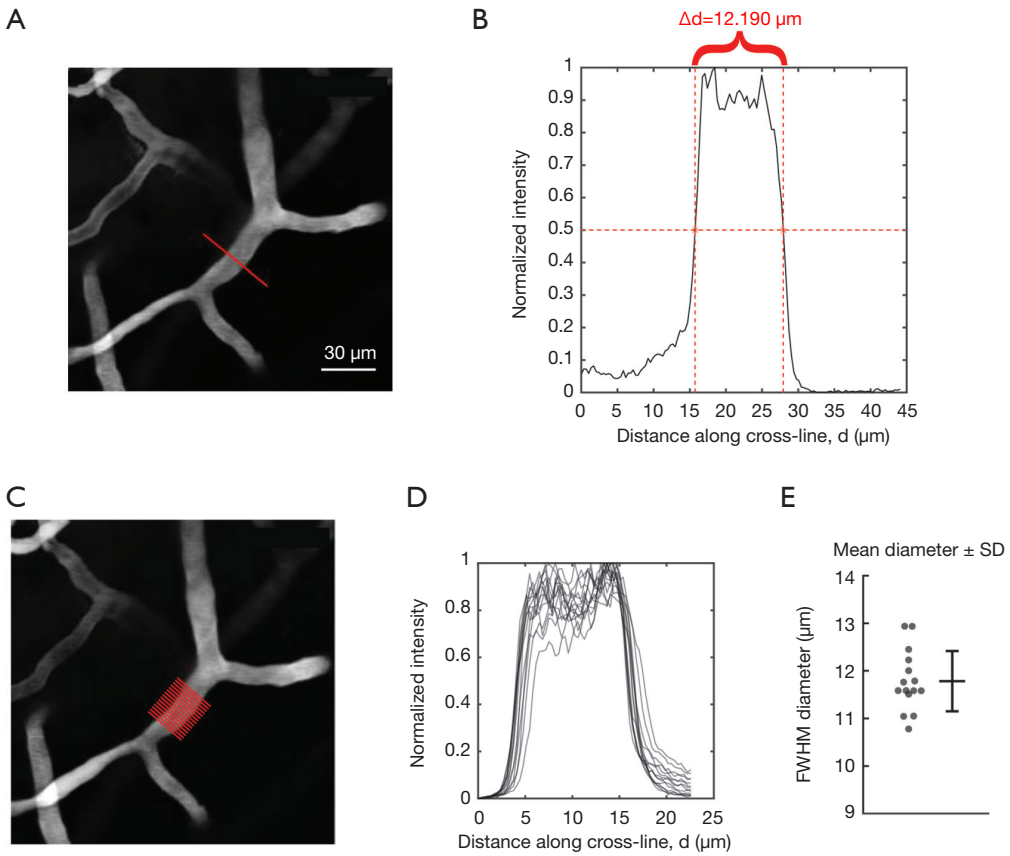

Figure 3 Full-width at half maximum diameter measurement. (A,B) A single cross-line placed over a pial arteriole. The normalized fluorescence intensity is plotted, and the width calculated as FWHM diameter is shown. (C,D,E) The process outlined in (A,B) is multiplexed with cross-lines created by VasoMetrics. Each cross-line provides a separate FWHM value, which can then be used to calculate the mean diameter and SD of the entire vessel segment (panel E). FWHM, full-width at half-maximum; SD, standard deviation.

the locations of half maximal fluorescence intensity are determined for both edges of the mesa. Pre-processing is performed by the code to improve the likelihood of identifying half-maximum locations nearest the center of the cross-line profile (see "Methods" section). The distance between these two points, or FWHM, provides an estimate of the lumen diameter (*Figure 3B*). This process is repeated with all cross-lines generated for a given through-line, providing a mean and error range for all measurements of width along the target vessel (*Figure 3C,D,E*). The program will output the diameter obtained on each cross-line in the columns of an ImageJ results table. If the image file is a movie, the process is further cycled through all image frames, where each row in the results table represents a frame. The processed results can be saved or manually copied and pasted into spreadsheet software for further data collation and analysis.

The cross-line locations are listed in the ROI manager (analyze > tools > ROI manager). In some cases, the user may wish to remove certain cross-lines due to their occurrence at vascular branchpoints or overlay on unwanted neighboring vessels that come in close contact with the measured vessel. These cross-lines can be removed by selecting the line in the ROI manager and clicking delete. The macro can then be rerun using the remaining ROI cross-lines to obtain a new mean diameter value. The cross-line positions for each through-line can be saved so that the user can return to them again in the future.

To test the accuracy of the FWHM approach in VasoMetrics, fluorescent microspheres (3.7 μm diameter verified by manufacturer) were imaged and their FWHM diameter measured by placing a short length of through-line such that only one cross-line was created along the midline of the sphere. The calculated diameter values were

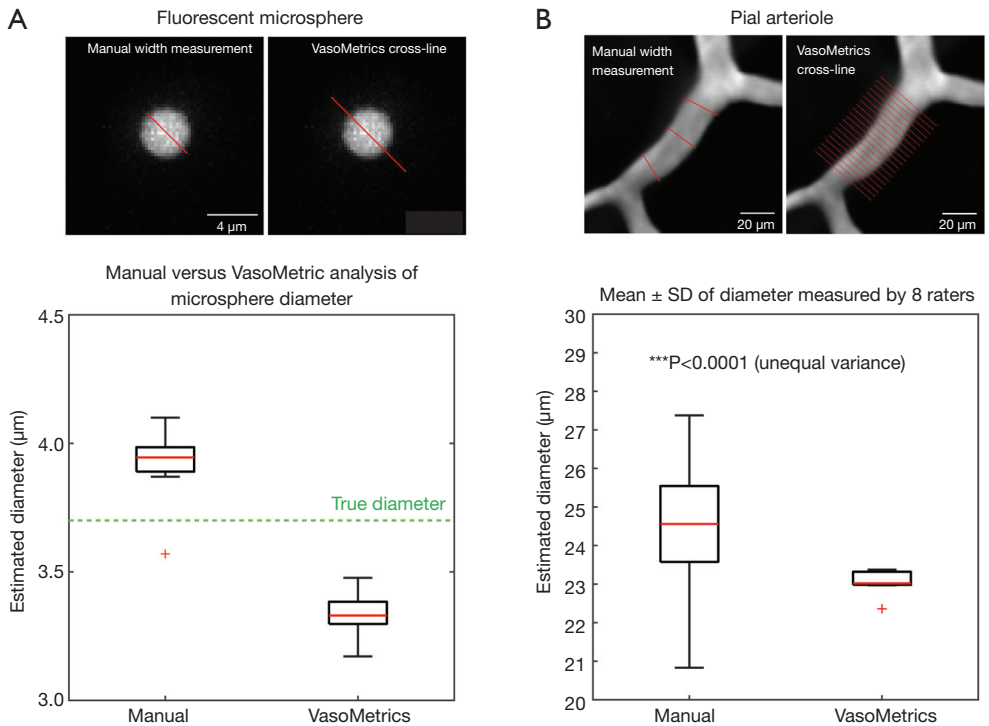

Figure 4 Increased accuracy and reduced user variability with VasoMetrics. (A) Accuracy of diameter measurement tested on microspheres of known size. (B) Comparison of manual versus VasoMetrics-based quantification of pial arteriole diameter. Manual measurements lead to significantly greater variance in results between 8 independent raters.

consistently very close to the true diameter, albeit with a small underestimation [3.34±0.08 µm; mean ± standard deviation (SD)]. This is expected because FWHM measures the diameter just before the loss of signal intensity at the edge of the microsphere. In comparison, manual measurement of microsphere diameter using the straight-line tool in ImageJ was also consistent, but slightly overestimated the true microsphere diameter (3.93±0.10 µm; mean ± SD) (*Figure 4A*). This is also expected because potential partial volume effects may make the microsphere appear larger.

We next compared vessel diameter measurements from *in vivo* data using either manual measurement or the VasoMetrics approach. We asked eight independent raters to measure the diameter of the same arteriole segment in a maximal projection image, both by hand using the straight-line tool in ImageJ/Fiji, or using VasoMetrics. No specific instruction was given as to where manual measurements should be collected, other than to take three separate measurements of diameter and to provide an average value. For VasoMetrics, raters were instructed to place the through-line from one end of the arteriole segment to the other, which generated 9 to 19 cross-lines spaced 5 µm and the average of these measurements was used for comparison. We found that inter-rater variance for arteriole diameter was high with manual measurements, in part because measurement line placements varied significantly. In contrast, diameter variance was significantly lower using VasoMetrics, even though through-line placements also varied slightly between raters (***P<0.0001, F-test of unequal variance) (*Figure 4B*). Altogether, these quality control tests show that VasoMetrics provides accurate and consistent measurements of vessel diameter in single image frames.

To test the ability to quantify vascular dynamics, we imaged pial vasculature in a mouse lightly sedated with chlorprothixene (*Figure 5A*). Tissue movement caused by breathing artifacts can cause vessels to shift slightly from the focal plane, which can appear as diameter changes during analysis. To avoid this, we captured sequential image stacks and quantified vessel diameter in maximally projected data. Image stacks were collected once every 17 seconds. A pial arteriole is found in the center of the image and two penetrating arteriole offshoots branch from this vessel. In total, four arteriole segments were measured, including

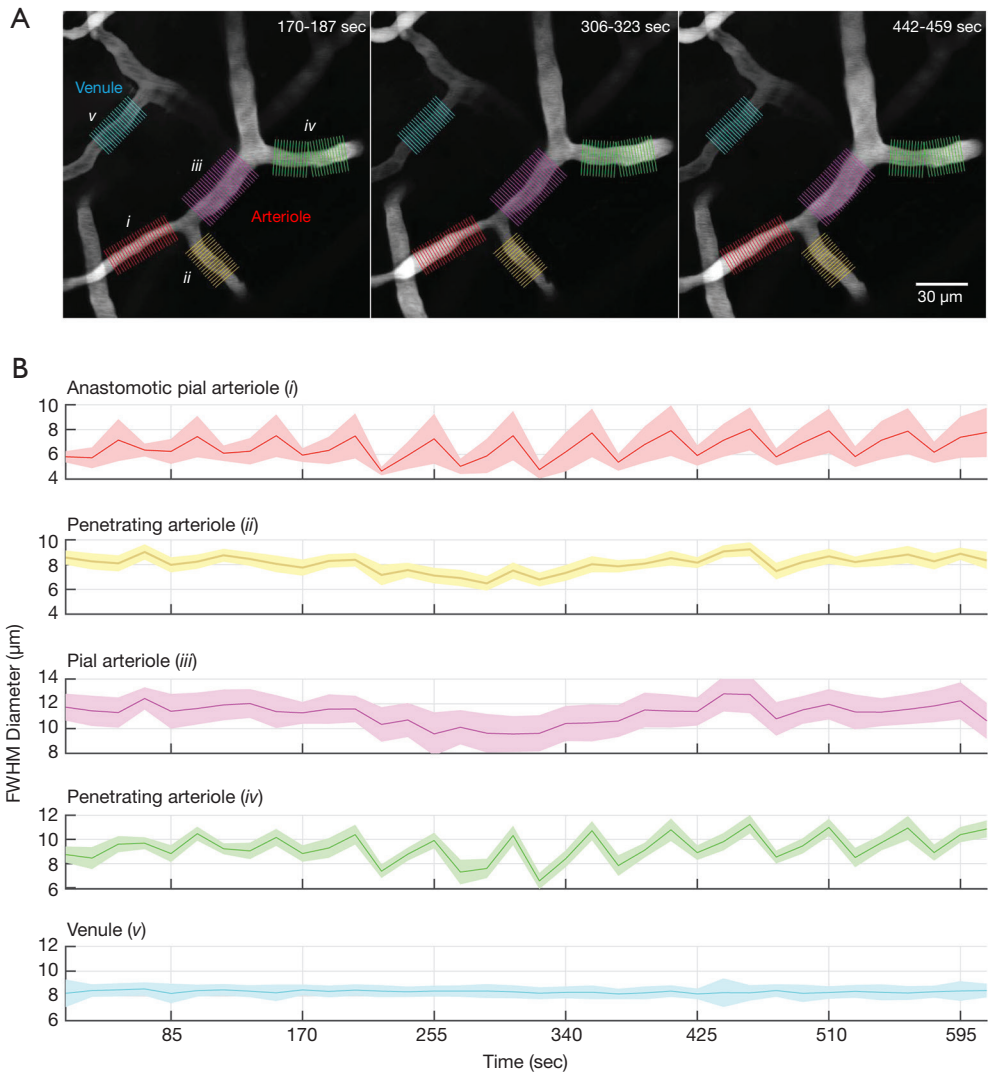

Figure 5 Detection of vasomotor oscillations in pial arterioles. (A) Pial arteriole and neighboring venule imaged with sequential image stacks collected every 17 seconds. Five separate vessel segments were analyzed using VasoMetrics. (B) Time-course plot for diameter (mean ± SD) of each vessel segment. SD, standard deviation.

two pial arteriole and two penetrating arteriole segments (*Figure 5B*). A neighboring venule was also measured as a control vessel for movement artifacts (3). Through-lines were between ~30–50 µm in length, which corresponded to 16 to 27 cross-lines per segment. We then plotted the average and SD of diameters from all cross-lines for each vessel segment examined. We detected very slow, oscillatory diameter changes occurring near 0.02 Hz for two of the arteriole segments, which corresponded to a penetrating arteriole offshoot (green) and a low flowing anastomotic segment (red). Curiously, the arteriole segments intervening these regions (yellow and purple) were more stable in diameter over the same time frame. In contrast, the neighboring venule exhibited no diameter change. This dataset demonstrates how VasoMetrics can be used to assess vascular diameter across different regions of a pial vascular network. While sampling rate was slow in this example, and aliasing of faster oscillatory rhythms may be occurring, the feasibility of processing movie stacks is demonstrated.

In a second example data set, we collected a long movie (single plane) of pial arterioles with acquisition at 0.78 Hz (*Figure 6*). This mouse was also lightly sedated by

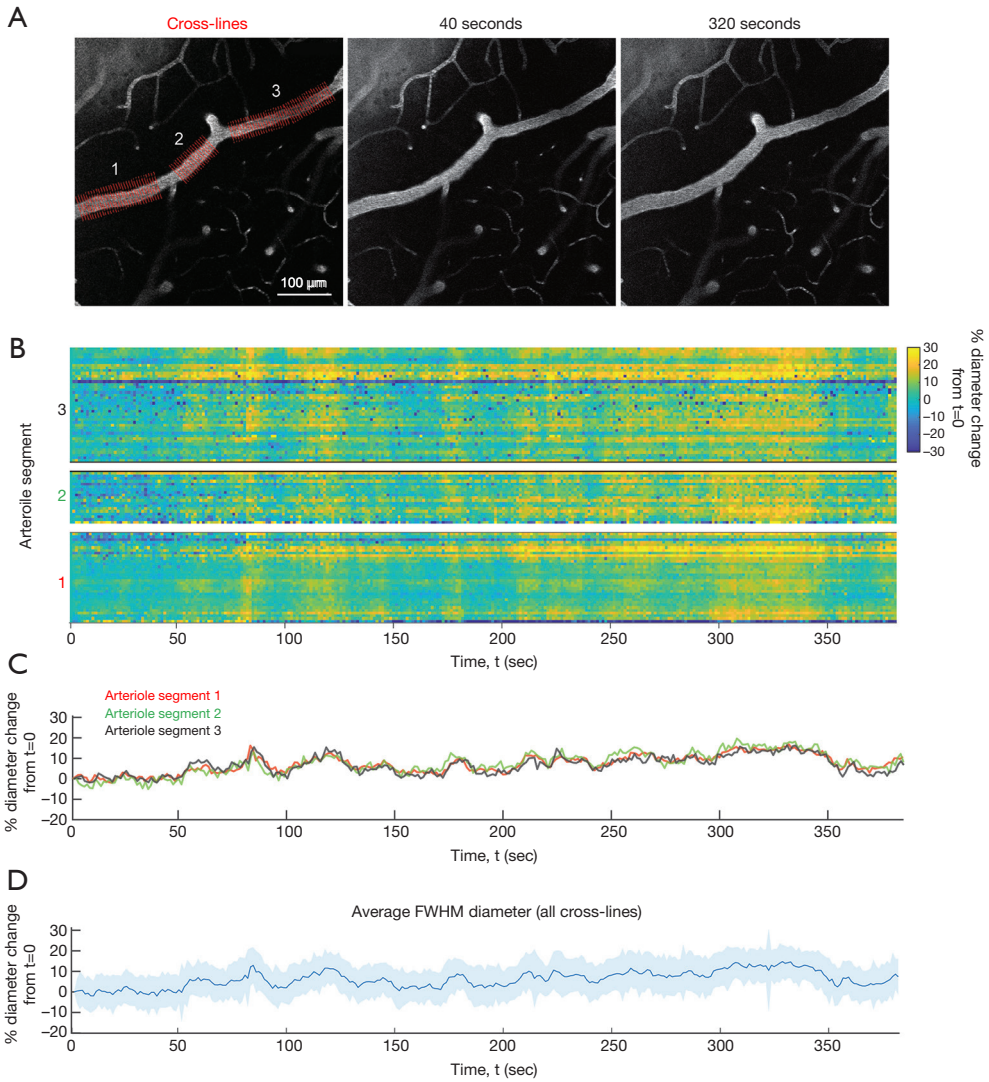

Figure 6 Detailed assessment of spatiotemporal dynamics in pial arterioles. (A) A long stretch of pial arteriole imaged at 0.78 Hz (single image plane). Three separate regions are sampled using VasoMetrics. (B) Space-time plot of change in arteriole diameter. (C,D) Time-course plot for diameter change of individual arteriole segments (C) and the entire arteriole, created by averaging results across all cross-lines (D); mean ± SD is plotted. SD, standard deviation.

chlorprothixene. We selected a long stretch of pial arteriole roughly 600 µm in length, with two short penetrating arteriole offshoots. Three through-lines were used to sample nearly the entire stretch of the pial arteriole (*Figure 6A*). This involved three separate data runs of VasoMetrics analysis. However, one can also use a single through-line and omit specific stretches of unwanted data in post-processing. Additionally, measurement of long vessels makes use of the multi-segment feature of VasoMetrics, where multiple through-lines can strung together to follow the trajectory of the target vessel (see "Methods" section). Altogether, the three through-lines involved 98 cross-lines with 5 µm spacing. Arteriole diameter was processed over 300 image frames corresponding to 385 seconds of data. The resulting matrix of data is plotted as a space-time image, revealing robust, periodic dilations that span the entire length of arteriole (*Figure 6B*). However, there is also some regional variation in diameter, which can be better appreciated in this form of data visualization. This data can further be collapsed down to provide the average

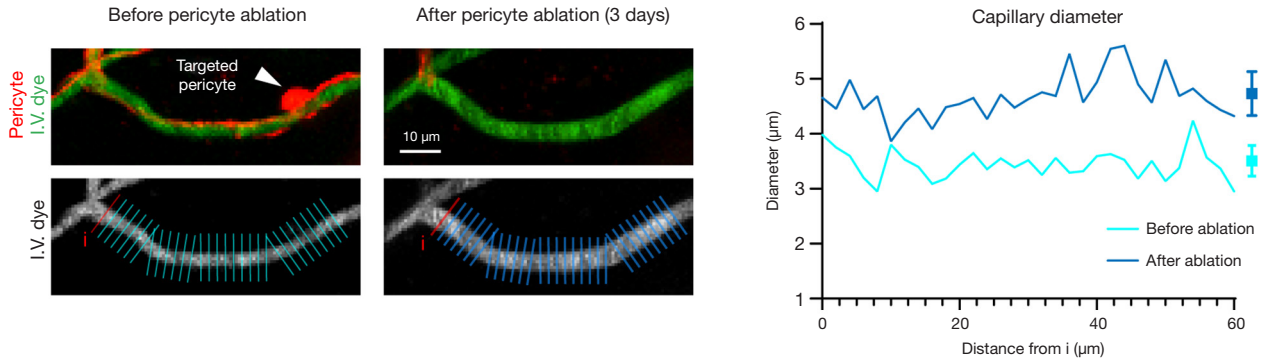

Figure 7 Detection of capillary diameter change following pericyte ablation. (A) Images collected from cerebral cortex of PDGFRβ-tdTomato mice showing a labeled pericyte on a capillary. The pericyte was ablated using focused laser irradiation at the cell soma. The capillary region newly devoid of pericyte contact dilates. (B) Capillary diameter before and after pericyte ablation, plotted as a function of distance from the cross-line shown in red. Mean diameter ± SD for all cross-lines is shown on the right of each graph. SD, standard deviation.

and SEM of diameter change for specific vessel segments, or the arteriole as a whole (*Figure 6C,D*). These oscillations may correspond to either basal vasomotor responses, or responses evoked by motor activity, as the cranial window was placed over sensorimotor cortex.

We next tested the sensitivity of VasoMetrics for detection of diameter changes in capillaries, which are typically no more than 4–6 µm in width in mouse cerebral cortex. In recent studies, we demonstrated that optical ablation of capillary pericytes led to sustained capillary dilation (21). We used this experimentally-induced change in capillary diameter to test VasoMetrics. In our example, a single capillary pericyte is ablated. An image stack is taken before and after the ablation, and maximal projections are created (*Figure 7A*). A multi-segmented through-line is used to address the curvature of the capillary. The capillary segment underlying the ablated pericyte is completely uncovered and dilates homogenously over the territory of the through-line. This pre-ablation and post-ablation diameter data can be plotted as a function of distance along the capillary (*Figure 7B*). These data show that capillary diameter can be analyzed using VasoMetrics, and that the fluorescence intensity profile across capillaries can be captured with adequate resolution for FWHM measurements.

We next assessed the ability to measure vascular diameter in data collected by other contrast-enhanced vascular imaging modalities. Optical coherence tomography angiography (OCTA) is used to study retinal microvascular networks and produces images with high contrast and resolution (23). We used VasoMetrics to quantify the diameter of arterioles in an image collected from superficial retina of a human patient with diabetic retinopathy using OCTA. The image shows arteriolar branches converging at the fovea, surrounded by capillaries (*Figure 8A*). The diameter of one arteriolar branch was measured with multiple through-lines, providing a total of 73 cross-lines. The FWHM diameter of each cross-line was calculated, revealing a broad range of diameters (25–45 µm range) and large SD, despite the vessel appearing of fairly even in caliber by eye (*Figure 8B,C*). A closer examination of diameter versus distance along an arteriole sub-region shows that diameter estimates are heterogeneous, and reflects either normal physiology or variations in signal detection (*Figure 8D*). Nevertheless, it is clear that a single measurement of width along this arteriole would not provide an adequate estimate of average diameter. That is, a measurement at the middle of the sub-region shown would result in a diameter 10–15% lower than the average. These data further indicate that VasoMetrics has utility in processing of clinical imaging data from the retina.

Discussion

We have shown that VasoMetrics is a robust, user-friendly macro for spatiotemporal analysis of vascular diameter in high-resolution, contrast-enhanced imaging applications such as two-photon microscopy and optical coherence tomography. VasoMetrics achieves highly reliable measures of diameter at multiple points along a vessel by using

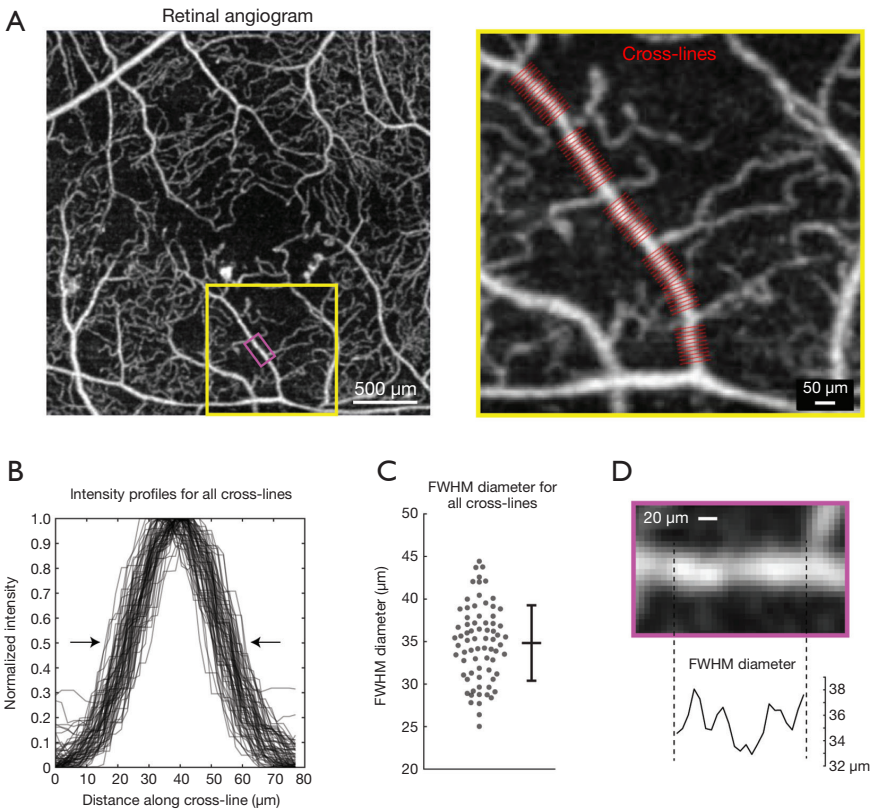

Figure 8 Measurement of arteriole diameter in the human retina. (A) Image of microvasculature surrounding the fovea collected from an adult male patient with diabetic retinopathy. Cross-line positions for the selected arteriole of interest are shown (inset). (B) Intensity profiles plotted as a function of distance along the cross-line for one arteriolar branch within the yellow inset region. (C) FWHM diameter calculated for each cross-line, along with mean ± SD. (D) A sub-region of the target arteriole shows heterogeneity in FWHM diameter along its length (purple inset). FWHM, full-width at half-maximum; SD, standard deviation.

existing image analysis features in the widely adopted ImageJ/Fiji software. This is a major advance over the standard approach, which is to obtain only a few diameters at user-defined points along the vessel, possibly creating biases and non-reproducibility in diameter measurements. A further improvement is that VasoMetrics can better quantify the heterogeneity of diameters along lengths of microvasculature that can arise during physiology and pathology. This feature is particularly important in characterizing the vascular responses to neural activation or in disease states involving mural cell pathology.

The importance of an unbiased, multi-location diameter measurement was recently highlighted by Ivanova *et al.* who sought to quantify heterogeneous capillary changes evoked by stimulation of pericytes in retinal vascular networks (15). The authors manually collected numerous diameter measurements along the capillary length in response to electrical stimulation of pericytes and application of vasoactive mediators. Their approach revealed how increasing pericyte stimulation intensity could promote propagative constriction along the capillary. This critical but laborious analysis may benefit from VasoMetrics if the vascular wall or intraluminal space could be labeled, as has been done with fluorescent IB4 (24), and intraluminal Evans Blue or similar fluorescent probes (25). In recent studies, we used VasoMetrics to quantify the average diameter of pre-capillary arterioles and capillaries in response to optical and genetic manipulation of pericytes *in vivo* (21,26,27). These prior studies only reported average diameter values obtained from VasoMetrics, but *Figure* 7 demonstrates how through- and cross-lines might be placed for such quantifications. In one instance, the variance in microvascular diameter was assessed (27). This analysis could only be performed using an approach with unbiases sampling of diameter along the

vessel length.

One limitation is that VasoMetrics does not handle measurement of vessel cross-section area, which is often collected for studies of neurovascular regulation below the brain surface. This type of data captures a cross-sectional slice of a penetrating arteriole as it descends into the cerebral cortex and takes on an ellipsoid cross-sectional shape (28-30). However, straightforward analysis routines involving image thresholding and particle analysis can be used to quantify area of fluorescence. Similarly, line-scan data is often collected for two-photon blood flow imaging applications. A specific location along the vessel is chosen a priori and the laser scan is cycled across the vessel width at this location with high frequency (~1 kHz) to extract vessel diameter. This is often coupled to line-scans parallel to the vessel lumen, for simultaneous capture of blood cell velocity (31,32). This approach is advantageous in that it provides very high sampling rates of vascular diameter that may be necessary to detect rapid onset of dilatory responses. However, it also has the potential for bias because the scan location must be predetermined, and responses may be overlooked if the scan location is incorrectly placed.

We envision that VasoMetrics will be useful for vascular data collected by multi-photon imaging. Imaging systems that collect 2-D or 3-D data with greater temporal frequency could lead to rich data sets of vascular spatiotemporal dynamics. However, the utility of VasoMetrics extends beyond pre-clinical imaging. We have also examined its utility in OCT angiography data, a clinical imaging modality that can be used, for instance, to measure vascular diameter or reactivity changes associated with diabetic retinopathy (33). We suspect that VasoMetrics can be further applied to other data types with contrast-enhanced vascular visualization with sufficient spatial resolution. Future studies could couple clinical imaging modalities (e.g., CT or digital subtraction angiography) with the study of vessel heterogeneity in vascular diseases such as diabetes, vasculitides, and vasospasm after subarachnoid hemorrhage. In fact, the width of any thin elongated object in a cross-sectional image could potentially be quantified using VasoMetrics. However, applications beyond multi-photon imaging and OCTA have not been tested in our hands, and we suggest use of ground truth controls with known object diameters to carefully test the validity of results obtained.

Acknowledgments

We are grateful to Prof. Ruikang Wang for providing the retinal angiogram image of *Figure 8*.

Funding: Our work is supported by grants to AYS from the NINDS and NIA (NS106138, AG063031, NS097775, AG062738). DAH is supported by a fellowship from NINDS (F30NS096868). AAB is supported by a scholarship from the American Federation for Aging Research.

Footnote

Provenance and Peer Review: With the arrangement by the Guest Editors and the editorial office, this article has been reviewed by external peers.

Conflicts of Interest: The authors have completed the ICMJE uniform disclosure form (available at http://dx.doi.org/10.21037/qims-20-920). The special issue "Advanced Optical Imaging in Biomedicine" was commissioned by the editorial office without any funding or sponsorship. The authors have no other conflicts of interest to declare.

Ethical Statement: This study was approved by The Institutional Animal Care and Use Committee at the Seattle Children's Research Institute.

References

1. Shih AY, Driscoll JD, Drew PJ, Nishimura N, Schaffer CB, Kleinfeld D. Two-photon microscopy as a tool to study blood flow and neurovascular coupling in the rodent brain. J Cereb Blood Flow Metab 2012;32:1277-309.
2. Iadecola C. The neurovascular unit coming of age: a journey through neurovascular coupling in health and disease. Neuron 2017;96:17-42.
3. Mateo C, Knutsen PM, Tsai PS, Shih AY, Kleinfeld D. Entrainment of arteriole vasomotor fluctuations by neural activity is a basis of blood-oxygenation-level-dependent "resting-state" connectivity. Neuron 2017;96:936-48.e3.
4. van Veluw SJ, Hou SS, Calvo-Rodriguez M, Arbel-Ornath

M, Snyder AC, Frosch MP, Greenberg SM, Bacskai BJ. Vasomotion as a driving force for paravascular clearance in the awake mouse brain. Neuron 2020;105:549-61.e5.
5. Li Y, Wei W, Wang RK. Capillary flow homogenization during functional activation revealed by optical coherence tomography angiography based capillary velocimetry. Sci Rep 2018;8:4107.
6. Gutiérrez-Jiménez E, Cai C, Mikkelsen IK, Rasmussen PM, Angleys H, Merrild M, Mouridsen K, Jespersen SN, Lee J, Iversen NK, Sakadzic S, Østergaard L. Effect of electrical forepaw stimulation on capillary transit-time heterogeneity (CTH). J Cereb Blood Flow Metab 2016;36:2072-86.
7. Jespersen SN, Østergaard L. The roles of cerebral blood flow, capillary transit time heterogeneity, and oxygen tension in brain oxygenation and metabolism. J Cereb Blood Flow Metab 2012;32:264-77.
8. Drew PJ, Shih AY, Kleinfeld D. Fluctuating and sensory-induced vasodynamics in rodent cortex extends arteriole capacity. Proc Natl Acad Sci U S A 2011;108:8473-8.
9. Schneider CA, Rasband WS, Eliceiri KW. NIH Image to ImageJ: 25 years of image analysis. Nat Methods 2012;9:671-5.
10. Driscoll JD, Shih AY, Drew PJ, Cauwenberghs G, Kleinfeld D. Two-photon imaging of blood flow in cortex. In: Helmchen F, Konnerth A, Yuste R. editors. Imaging in neuroscience: a laboratory manual. New York: Cold Spring Harbor Laboratory Press, 2011:927-38.
11. Hill RA, Tong L, Yuan P, Murikinati S, Gupta S, Grutzendler J. Regional blood flow in the normal and ischemic brain is controlled by arteriolar smooth muscle cell contractility and not by capillary pericytes. Neuron 2015;87:95-110.
12. Sekiguchi Y, Masamoto K, Takuwa H, Kawaguchi H, Kanno I, Ito H, Tomita Y, Itoh Y, Suzuki N, Sudo R, Tanishita K. Measuring the vascular diameter of brain surface and parenchymal arteries in awake mouse. Adv Exp Med Biol 2013;789:419-25.
13. Devor A, Tian P, Nishimura N, Teng IC, Hillman EM, Narayanan SN, Ulbert I, Boas DA, Kleinfeld D, Dale AM. Suppressed neuronal activity and concurrent arteriolar vasoconstriction may explain negative blood oxygenation level-dependent signaling. J Neurosci 2007;27:4452-9.
14. Peppiatt CM, Howarth C, Mobbs P, Attwell D. Bidirectional control of CNS capillary diameter by pericytes. Nature 2006;443:700-4.
15. Ivanova E, Kovacs-Oller T, Sagdullaev BT. Vascular pericyte impairment and connexin43 gap junction deficit contribute to vasomotor decline in diabetic retinopathy. J Neurosci 2017;37:7580-94.
16. Madisen L, Zwingman TA, Sunkin SM, Oh SW, A. ZH, Gu H, Ng LL, Palmiter RD, Hawrylycz MJ, Jones AR, Lein ES. A robust and high-throughput Cre reporting and characterization system for the whole mouse brain. Nat Neurosci 2010;13:133-40.
17. Cuttler AS, LeClair RJ, Stohn JP, Wang Q, Sorenson CM, Liaw L, Lindner V. Characterization of Pdgfrb-Cre transgenic mice reveals reduction of ROSA26 reporter activity in remodeling arteries. Genesis 2011;49:673-80.
18. Hartmann DA, Underly RG, Grant RI, Watson AN, Lindner V, Shih AY. Pericyte structure and distribution in the cerebral cortex revealed by high-resolution imaging of transgenic mice. Neurophotonics 2015;2:041402.
19. Drew PJ, Shih AY, Driscoll JD, Knutsen PM, Davalos D, Blinder P, Akassoglou K, Tsai PS, Kleinfeld D. Chronic optical access through a polished and reinforced thinned skull. Nat Methods 2010;7:981-4.
20. Shih AY, Mateo C, Drew PJ, Tsai PS, Kleinfeld D. A polished and reinforced thinned-skull window for long-term imaging of the mouse brain. J Vis Exp 2012;(61):3742.
21. Berthiaume AA, Grant RI, McDowell KP, Underly RG, Hartmann DA, Levy M, Bhat NR, Shih AY. Dynamic remodeling of pericytes in vivo maintains capillary coverage in the adult mouse brain. Cell Rep 2018;22:8-16.
22. Berthiaume AA, Hartmann DA, Majesky MW, Bhat NR, Shih AY. Pericyte Structural Remodeling in Cerebrovascular Health and Homeostasis. Front Aging Neurosci 2018;10:210.
23. Chen CL, Wang RK. Optical coherence tomography based angiography [Invited]. Biomed Opt Express 2017;8:1056-82.
24. Mishra A, O'Farrell FM, Reynell C, Hamilton NB, Hall CN, Attwell D. Imaging pericytes and capillary diameter in brain slices and isolated retinae. Nat Protoc 2014;9:323-36.
25. Kovacs-Oller T, Ivanova E, Bianchimano P, Sagdullaev BT. The pericyte connectome: spatial precision of neurovascular coupling is driven by selective connectivity maps of pericytes and endothelial cells and is disrupted in diabetes. Cell Discov 2020;6:39.
26. Hartmann DA, Berthiaume AA, Grant RI, Harrill SA, Noonan T, Costello J, Tieu T, McDowell K, Faino A, Kelly A, Shih AY. Brain capillary pericytes exert a substantial but slow influence on blood flow. bioRXiv 2020. Available online: https://doi.org/10.1101/2020.03.26.008763

27. Watson AN, Berthiaume AA, Faino AV, McDowell KP, Bhat NR, Hartmann DA, Shih AY. Mild pericyte deficiency is associated with aberrant brain microvascular flow in aged PDGFRβ+/- mice. J Cereb Blood Flow Metab 2020;40:2387-400.
28. Petzold GC, Albeanu DF, Sato TF, Murthy VN. Coupling of neural activity to blood flow in olfactory glomeruli is mediated by astrocytic pathways. Neuron 2008;58:897-910.
29. Tian P, Teng I, May LD, Kurz R, Lu K, Scadeng M, Hillman EM, De Crespigny AJ, D'Arceuil HE, Mandeville JB, Marota JJ, Rosen BR, Lui TT, Boas DA, Buxton RB, Dale AM, Devor A. Cortical depth-specific microvascular dilation underlies laminar differences in blood oxygenation level-dependendent functional MRI signal. Proc Natl Acad Sci U S A 2010;107:15246-51.
30. Tran CHT, Peringod G, Gordon GR. Astrocytes integrate behavioral state and vascular signals during functional hyperemia. Neuron 2018;100:1133-48.e3.
31. Driscoll JD, Shih AY, Drew PJ, Cauwenberghs G, Kleinfeld D. Two-photon imaging of blood flow in the rat cortex. Cold Spring Harb Protoc 2013;2013:759-67.
32. Rungta RL, Chaigneau E, Osmanski BF, Charpak S. Vascular compartmentalization of functional hyperemia from the synapse to the pia. Neuron 2018;99:362-375.e4.
33. Heitmar R, Lip GYH, Ryder RE, Blann AD. Retinal vessel diameters and reactivity in diabetes mellitus and/or cardiovascular disease. Cardiovasc Diabetol 2017;16:56.

Cite this article as: McDowell KP, Berthiaume AA, Tieu T, Hartmann DA, Shih AY. VasoMetrics: unbiased spatiotemporal analysis of microvascular diameter in multi-photon imaging applications. Quant Imaging Med Surg 2021;11(3):969-982. doi: 10.21037/qims-20-920